AIP | Physics of Fluids

Lift enhancement by dynamically changing wingspan in forward flapping flight

Shizhao Wang, Xing Zhang, Guowei He, and Tianshu Liu

Citation: Physics of Fluids (1994-present) **26**, 061903 (2014); doi: 10.1063/1.4884130
View online: http://dx.doi.org/10.1063/1.4884130
View Table of Contents: http://scitation.aip.org/content/aip/journal/pof2/26/6?ver=pdfcov
Published by the AIP Publishing

PHYSICS OF FLUIDS **26**, 061903 (2014)

Lift enhancement by dynamically changing wingspan in forward flapping flight

Shizhao Wang,[1] Xing Zhang,[1] Guowei He,[1,a)] and Tianshu Liu[2]
[1]*The State Key Laboratory of Nonlinear Mechanics, Institute of Mechanics, Chinese Academy of Sciences, Beijing 100190, People's Republic of China*
[2]*Department of Mechanical and Aerospace Engineering, Western Michigan University, Kalamazoo, Michigan 49008, USA*

(Received 22 January 2014; accepted 27 May 2014; published online 24 June 2014)

Dynamically stretching and retracting wingspan has been widely observed in the flight of birds and bats, and its effects on the aerodynamic performance particularly lift generation are intriguing. The rectangular flat-plate flapping wing with a sinusoidally stretching and retracting wingspan is proposed as a simple model for biologically inspired dynamic morphing wings. Numerical simulations of the low-Reynolds-number flows around the flapping morphing wing are conducted in a parametric space by using the immersed boundary method. It is found that the instantaneous and time-averaged lift coefficients of the wing can be significantly enhanced by dynamically changing wingspan in a flapping cycle. The lift enhancement is caused by both changing the lifting surface area and manipulating the flow structures responsible to the vortex lift generation. The physical mechanisms behind the lift enhancement are explored by examining the three-dimensional flow structures around the flapping wing.
 [http://dx.doi.org/10.1063/1.4884130]

I. INTRODUCTION

Animal flight has provided inspirations for new designs of Micro Aerial Vehicles (MAVs), since natural flyers usually have the extraordinary maneuvering capability, high lift, and efficient propulsion. On the other hand, the complex low-Reynolds-number unsteady aerodynamics in flapping flight poses challenges to researchers in aerodynamics and fluid mechanics because the knowledge and database of the design of fixed-wing aircraft are not suitable in the design of such MAVs. Therefore, it is desirable to understand the physical mechanisms of lift generation in animal flight. Insects, birds, and bats are the three groups of extant flying animals. Notwithstanding the different morphology and kinematics of their wings, the high-lift-generating mechanisms of flapping wings at low Reynolds numbers are the common merits of these flyers. Some unique mechanisms for enhancing the lift particularly in insect flight have been identified, including the "clap and fling" mechanism,[1,2] stable attached leading-edge vortex (LEV) during dynamic stall,[3–7] rapid acceleration of the wing at the beginning of a stroke, fast pitching-up rotation of the wing near the end of the stroke,[8] wake capture mechanism,[9,10] and wing-body/wing interaction.[11–13]

The aerodynamic force acting on flapping wings is directly related to the flow structures around the wings. The flow structures near wings and in the wakes have been extensively investigated by measuring flow fields around natural flyers or mechanical models[3,14–19] and by numerical simulations.[4] The flow structures around a heaving and/or pitching rigid wing with several planforms as a simplified flapping wing were also investigated,[20–25] providing a useful understanding into low-Reynolds-number unsteady flows of animal flight. The comprehensive reviews on this topic are given in Refs. 26–30. Recently, the concept of flexible wings has been proposed, and flexible

[a)]Author to whom correspondence should be addressed. Electronic mail: hgw@lnm.imech.ac.cn. Telephone: 86-10-82543969.

wings of natural flyers could be adopted to improve the aerodynamic performance of MAVs. Insects usually have flexible membrane wings that deform elastically during flapping flight and modify the flow around the wings. Birds have flexible feathers, and bats have elastic membrane wings. The effects of the wing flexibility have attracted considerable attentions.[31–36]

More significantly, in contrast to insects, the wingspan and wing planform are actively changed though the motion of the skeleton structure in the flight of birds and bats.[16–18,37] This dynamic wing morphing is ubiquitous in the flight of birds and bats. For example, a bat wing has a bone skeleton with more than ten joints and therefore a bat can quickly change the wingspan and planform by moving the joints in a controllable way. In general, a bat (or bird) wing stretches outward in the downstroke and retracts inward in the upstroke. The ratio between the minimum and maximum wingspans of a Pallas' long tongued bat could be as low as 0.6.[38] The current research of morphing wings has been limited on steady and quasi-steady morphing to meet specified mission requirements at different flight regimes (such as takeoff, landing, and cruising).[39] The potential of the dynamic morphing of a flapping wing for improving the flight performance has not been explored.

For a dynamic morphing flapping wing with the time-dependent wing area, the lift coefficient in forward flight is defined as

$$Cl(t) = \frac{F_z(t)}{q_\infty S(t)}, \tag{1}$$

where F_z is the lift acting on the wing, $q_\infty = 0.5\rho U_\infty^2$ is the dynamical pressure, U_∞ is the freestream velocity (or forward flight velocity), and $S(t)$ is the instantaneous wing area. Theoretically, the effect of changing the wing area is removed in $Cl(t)$ since $S(t)$ is used for normalization. The time-averaged lift over a flapping period T is given by

$$\langle F_z \rangle_T = q_\infty T^{-1} \int_0^T Cl(t)S(t)dt, \tag{2}$$

where $\langle \bullet \rangle_T = T^{-1} \int_0^T \bullet \, dt$ is the time-averaging operator in a period T. According to Eq. (2), even when the time-averaged lift coefficient is zero, i.e., $\langle Cl \rangle_T = 0$, the positive time-averaged lift ($\langle F_z \rangle_T > 0$) could be still generated by dynamically changing the wing area in flapping flight as long as there is a positive correlation $\langle Cl(t)S(t) \rangle_T > 0$. The flight of birds and bats is just a good example in which the wing area is increased in the downstroke and decreased in the upstroke to generate the lift.

It is clear that the effect of changing the lifting surface area will directly alter the lift generation. There are few studies on the complex flows around a dynamic morphing flapping wing like a bat or bird wing. The flow structures altered by the dynamic morphing and their effects on the lift coefficient are not well understood. To gain a better understanding into this problem, a canonical morphing flapping wing, a rectangular flat-plate wing with a dynamically stretching and retracting wingspan, is considered. This simplified model characterizes the main spanwise morphing features of flapping wings of birds and bats although various birds and bats have more complex wing planforms and kinematics. The fundamental question is how dynamically stretching and retracting wingspan in a flapping cycle alters the flow structures and affects the lift as a result.

The objective of this work is to demonstrate through numerical simulations that the dynamic morphing of a flapping wing can enhance the lift and explore the physical mechanisms behind the lift enhancement. The strategy of solving this problem is outlined as follows. First, a generic dynamic morphing flapping wing model is proposed, which captures the main morphing features of a bird or bat wing in terms of stretching and retracting wingspan in flapping flight. This model is a rectangular flat-plate wing with a sinusoidally varying wingspan that reaches the maximum during the downstroke and the minimum during the upstroke. The wing geometry and kinematics are described and the relevant aerodynamic parameters are defined to evaluate the lift enhancement in Sec. II. The numerical method and setting are also briefly described in Sec. II. In Sec. III, the lift enhancement is examined in the parametric space and it is indicated that the lift can be significantly enhanced by both changing the lifting surface area and altering the flow structures in the process of stretching and retracting wingspan. Further, the vortical structures that are responsible to the

lift enhancement due to stretching and retracting wingspan are identified in Sec. IV. It is observed that the LEVs on the upper surface in the upstroke are significantly intensified and the shorter and weaker LEVs occur on the lower surface in both the upstroke and downstroke. These flow structures contribute to the overall vortex lift enhancement. These observations are further examined through a detailed data analysis based on the lift decomposition into the vortex lift (the Lamb vector integral) and the local acceleration term in Sec. V. Finally, the conclusions are drawn in Sec. VI.

II. MODEL AND METHOD

A. Generic morphing flapping wing

The geometry and kinematics of wings of flying birds and bats are complicated.[16–18,37] Therefore, to gain a clear understanding of the aerodynamics of a dynamic morphing flapping wing, the wing geometry and kinematics should be suitably simplified while the main morphing features of the wing are retained. A generic morphing flapping wing is proposed, as illustrated in Fig. 1, which characterizes the main features of dynamically stretching and retracting wingspan. A rectangular flat-plate wing with a constant geometrical angle of attack (AoA) α heaves harmonically in a uniform freestream flow. Meanwhile, its wingspan stretches outward before reaching a certain position in the downstroke and retracts inward to the center line before reaching a certain position in the upstroke. The wing thickness is zero, and the wing chord remains constant. The flapping kinematics is described in a fixed laboratory coordinate system, as shown in Fig. 1. The x-axis points downstream in the direction of the freestream flow, the y-axis is in the spanwise direction, and the z-axis is in vertical direction pointing upward. The flapping kinematics of the center of the wing is prescribed by

$$z_w = A\sin(2\pi f t), \tag{3}$$

where z_w is the vertical position of the wing center, A is the heaving amplitude, f is the flapping frequency. The flapping Strouhal number is defined as $St = 2fA/U_\infty$. The time history of z_w is shown in Fig. 2, where $T^* = t/T - 1/4 = ft - 1/4$ is a non-dimensional time in which the time is shifted by 1/4 of the period such that the downstroke in the flapping motion given by Eq. (3) starts at $T^* = 0$, 1, 2, $\cdots$ when z_w reaches the maximum.

The spanwise stretching and retracting motion of the wing has the same frequency as that of the flapping motion. The wingspan L reaches the maximum in the downstroke and the minimum in the upstroke. The wing aspect ratio (AR) is prescribed as a function of time, i.e.,

$$AR(t) = \frac{L}{c} = AR_0(a - b\sin(2\pi f t + \phi)), \tag{4}$$

where $AR_0 = L_0/c$ is the characteristic aspect ratio, L_0 is the characteristic wingspan, c is the constant chord, a and b are the coefficients that specify the stretching and retracting amplitude, and ϕ is the phase difference between the flapping and stretching/retracting motions. The time-averaged AR in

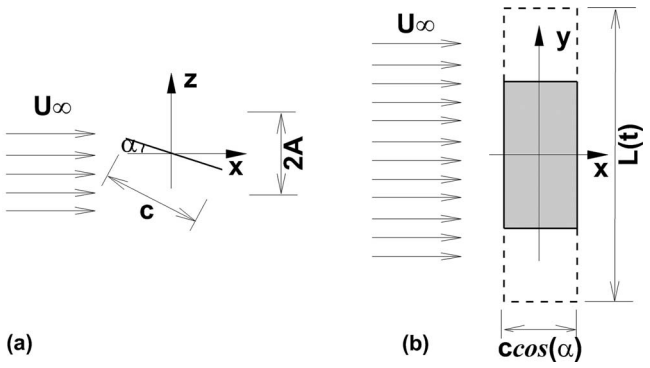

FIG. 1. Schematic of the computational model: (a) side view and (b) top view.

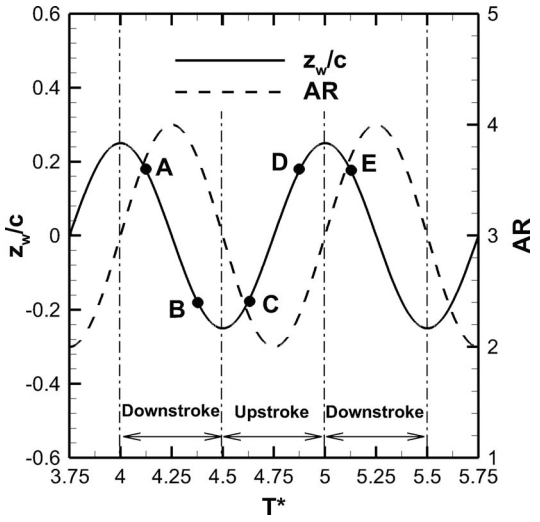

FIG. 2. The time histories of the vertical displacement of the wing and the aspect ratio in the case of $SR = 0.5$. The solid circles A, B, C, D, and E denote five key moments $T^* = 4.125$, 4.375, 4.625, 4.875, and 5.125, respectively, for illustration of the flow structures in Sec. IV.

a period is $\langle AR\rangle_T = aAR_0$. The span ratio, which is defined as a ratio between the minimum and maximum wingspans ($L_{\min}$ and $L_{\max}$), is introduced to measure the magnitude of the stretching and retracting wingspan, i.e.,

$$SR = \frac{L_{\min}}{L_{\max}}. \tag{5}$$

The span ratio depends on a and b for a given value of AR_0, as shown in Table I.

The time history of AR for $SR = 0.5$ and $\phi = \pi/2$ is shown in Fig. 2 along with the history of z_w/c. When the non-dimensional variables as $z_w^* = z_w/c$, $A^* = A/c$, $f^* = fc/U_\infty$, $t^* = tU_\infty/c$, $L_0^* = L_0/c$ are used, the non-dimensional forms of Eqs. (3) and (4) remain the same, which will be used in Secs. II B–V. In summary, there are the four kinematical parameters: the span ratio SR, the phase difference ϕ, the flapping Strouhal number $St = 2fA/U_\infty$, and the relative flapping magnitude $A^* = A/c$. The geometrical AoA α and the characteristic aspect ratio AR_0 are the other relevant parameters. The instantaneous wing area is $S(t) = L(t)c = c^2AR(t)$, and the time-averaged wing area in a period is $\langle S(t)\rangle_T = ac^2AR_0$.

B. Aerodynamic parameters

The overall lift enhancement of the morphing wing is affected by both the dynamic change of the lifting surface area and the altered flow structures by the dynamic morphing. A term "the

TABLE I. Coefficients specifying the amplitude of stretching and retracting wingspan.

SR	a	b	AR_0	$\langle AR\rangle_T$
0.25	0.625	0.375	4.0	2.5
0.375	0.6875	0.3125	4.0	2.75
0.5	0.75	0.25	4.0	3.0
0.6	0.8	0.2	4.0	3.2
0.7	0.85	0.15	4.0	3.4
0.75	0.875	0.125	4.0	3.5
0.8	0.9	0.1	4.0	3.6
0.85	0.925	0.075	4.0	3.7
0.9	0.95	0.05	4.0	3.8
1.0	1.0	0.0	4.0	4.0

effect of the morphing-altered flow structures" is used hereafter, which is defined as the additional effect induced by the dynamic morphing on the lift enhancement after the geometrical effect of the changing wing area is excluded. It will be pointed out later that the evolution of the LEVs is altered by the dynamic morphing and the effect of the morphing-altered flow structures is related to the vortex lift associated with the LEVs.

To characterize the overall lift enhancement, the lift coefficient based on the time-averaged wing area $\langle S\rangle_T$ is introduced, i.e.,

$$Cl_0(t) = \frac{F_z(t)}{q_\infty \langle S\rangle_T}. \tag{6}$$

The net increment of $Cl_0(t)$ is

$$\Delta Cl_0(t) = Cl_0(t) - Cl_{0,ref}(t), \tag{7}$$

where $Cl_{0,\,ref}(t)$ is the reference lift coefficient of a reference flapping wing with the fixed wingspan while the other parameters remain the same. This reference flapping wing has the fixed AR that equals to the time-averaged AR (i.e., $\langle AR\rangle_T = aAR_0$) of the corresponding dynamic morphing wing. Essentially, $\Delta Cl_0(t)$ represents the lift increment generated by both the effect of changing the wing area and the effect of the flow structures altered by the dynamic morphing. In contrast, the instantaneous lift coefficient $Cl(t)$ defined in Eq. (1) isolates the effect associated with the dynamic morphing by using the instantaneous wing area $S(t)$ for normalization. Similarly, to compare the wings with the dynamically changing wingspan and the fixed wingspan, the increment of $Cl(t)$ is given by

$$\Delta Cl(t) = Cl(t) - Cl_{ref}(t), \tag{8}$$

where $Cl_{ref}(t)$ is the reference lift coefficient of the reference flapping wing with the fixed wingspan and the aspect ratio of $\langle AR\rangle_T$. In fact, $Cl_{ref}(t) = Cl_{0,\,ref}(t)$ since the wing area is fixed for the reference wing. Here, $\Delta Cl(t)$ mainly represents the lift increment generated by the effect of the morphing-altered flow structures. Furthermore, both $\Delta Cl_0(t)$ and $\Delta Cl(t)$ depend on the parameters SR, ϕ, St, A^*, and α. The time-averaged quantity $\langle \Delta Cl_0\rangle_T$ represents the overall lift enhancement, while $\langle \Delta Cl\rangle_T$ describes the time-averaged lift enhancement caused by the effect of the morphing-altered flow structures when the effect of changing wing area is removed. In this paper, both $\langle \Delta Cl_0\rangle_T$ and $\langle \Delta Cl\rangle_T$ are used as the measures of the lift enhancement in the parametric space (SR, ϕ, St, A^*, α). A proportional relation is $\langle Cl\rangle_T = C_{FS}\langle Cl_0\rangle_T$, where the correlation coefficient is defined as $C_{FS} = \langle F_z(t)S^{-1}(t)\rangle_T \langle F_z\rangle_T^{-1}\langle S\rangle_T$.

C. Numerical method and settings

The flow around the flapping rectangular wing is governed by the incompressible Navier-Stokes (NS) equations

$$\begin{aligned} &\nabla \cdot \boldsymbol{u} = 0, \\ &\frac{\partial \boldsymbol{u}}{\partial t} + \boldsymbol{u}\cdot\nabla\boldsymbol{u} = -\nabla p + \frac{1}{\mathrm{Re}}\nabla^2\boldsymbol{u} + \boldsymbol{f}, \end{aligned} \tag{9}$$

where $\boldsymbol{u}$ is the non-dimensional velocity normalized by U_∞, p is the non-dimensional pressure normalized by ρU_∞^2, $\boldsymbol{f}$ is the non-dimensional body force in the immersed boundary (IB) method,[40,41] and $Re = U_\infty c/\nu$ is the Reynolds number. The unsteady flow with a moving boundary is handled by using a semi-implicit IB method in the frame work of discrete stream function formula.[42] With this method, the geometry and kinematics of the flapping wing are described by a set of the Lagrangian grid points. The NS equations are solved on a Cartesian grid by using the discrete stream function (or exact projection) approach, in which the divergence-free condition is exactly satisfied.[43] The detailed descriptions of the numerical method can be found in the work of Wang and Zhang.[42]

The present work focuses on the effect of dynamically changing wingspan. The Reynolds number is fixed at 300 for all the cases. This relatively low Reynolds number is selected by considering the following factors. First, the dynamically changing wingspan is observed in a wide range of

Reynolds numbers from several hundreds to about 10^5, such as in the slow-flying small bats (Pallas long-tongued bat) and seagulls. It is assumed that the effect of dynamically changing wingspan would be intrinsic and it could not be sensitive to the Reynolds number. Furthermore, the flapping rectangular wing used in the present work has a sharp leading edge. The flow separates immediately at the leading edge, and the separation point is not sensitive to the Reynolds number. In most cases, the characteristic aspect ratio is fixed at $AR_0 = 4$. The flapping rectangular wing with $SR = 0.5$, $St = 0.3$, $A^* = 0.25$, and $\alpha = 0^\circ$ is selected as a typical case. The lift enhancement of the dynamic morphing flapping wing is investigated in the parametric space (SR, ϕ, St, A^*, α). A non-dimensional computational domain of $[-16, 34] \times [-15, 15] \times [-15, 15]$ in the streamwise, spanwise, and vertical directions is used. The uniform freestream flow is specified at the inlet of the computational domain. The free convection boundary condition is set at the outlet. The no-slip boundary condition is satisfied on the surface of the flapping wing. The zero-shear slip wall (no-friction) condition is imposed on the other boundaries. The flow is uniform with (1, 0, 0) at $t = 0$, and the flapping wing appears at $t = 0^+$.

An unstructured Cartesian grid, with local refinement using hanging nodes, is used to discretize the computational domain. The total number of discrete cells is 10 189 700 with the grid size $\delta h/c = 0.02$ in a refined domain of $[-1, 1] \times [-3, 3] \times [-1, 1]$ around the flapping wing, $\delta h/c = 0.04$ in a region of $[-2, 8] \times [-4, 4] \times [-2, 2]$ to resolve the flow structures in the wake, and $\delta h/c \leq 0.32$ in the far field. The Lagrangian grid size varies with time in a range from the minimum of $\delta s/c = 0.01$ to the maximum of $\delta s/c = 0.02$. Additional simulations are conducted to ensure that the reasonable converged results are achieved in this work when the minimum grid size of $\delta h/c = 0.02$ and time step of $\Delta t^* < 0.005$ are used. The code validation in various unsteady flows is described by Wang and Zhang.[42]

III. LIFT ENHANCEMENT

The lift acting on the flapping wing with the stretching and retracting wingspan depends on the span ratio (SR), phase difference (ϕ), Strouhal number (St), relative flapping amplitude (A^*), and geometrical AoA (α). To examine the lift enhancement, the lift coefficients $Cl_0(t)$ and $Cl(t)$ are calculated, and the time-averaged lift coefficient increments $\langle \Delta Cl_0 \rangle_T$ and $\langle \Delta Cl \rangle_T$ are evaluated in the parametric space (SR, ϕ, St, A^*, α) for $AR_0 = 4$. The effect of the span ratio (SR) on the lift enhancement is first investigated in Subsection III A and then the effects of the other parameters (ϕ, St, A^*, α) are examined in Subsection III B.

A. Effect of span ratio

We consider a typical case of the flapping wing with the stretching and retracting wingspan, where the kinematical and geometrical parameters are (SR, ϕ, St, A^*, α) = (0.5, $\pi/2$, 0.3, 0.25, 0°) (referred to as the case of $SR = 0.5$) for $AR_0 = 4$. For comparison, the corresponding wing with the fixed wingspan and $AR = 3$ is considered, where (SR, ϕ, St, A^*, α) = (1.0, $\pi/2$, 0.3, 0.25, 0°) (referred to as the case of $SR = 1.0$). Figure 3(a) shows the time histories of $Cl_0(t)$ and $Cl(t)$ in the cases of $SR = 0.5$ and $SR = 1.0$. Overall, both the lift coefficients $Cl_0(t)$ and $Cl(t)$ for $SR = 0.5$ are larger than those for $SR = 1.0$ during the most time of a flapping cycle. This observation indicates that the stretching and retracting wingspan motion can enhance the time-averaged lift. Further, since the effect of changing wing area is removed in $Cl(t)$, the fact that $Cl(t)$ for $SR = 0.5$ is larger than that for $SR = 1.0$ implies that the effect of the morphing-altered flow structures is responsible to the lift enhancement in addition to the effect of changing lifting surface area.

In the case of $SR = 0.5$, the maximum of $Cl_0(t)$ is reached when the wing is at about 1/3 of the downstroke. At the beginning of the upstroke, $Cl_0(t)$ is at the minimum. The maximum magnitude of the positive $Cl_0(t)$ generated in the downstroke is about two times larger than that of the negative $Cl_0(t)$ in the upstroke. This asymmetric lift generation in the downstroke and upstroke results in $\langle Cl_0 \rangle_T > 0$. In the case of $SR = 1.0$ where the wingspan remains constant during a flapping cycle, $Cl_0(t)$ reaches the maximum when the wing moves about 1/3 of the downstoke. The lift generation

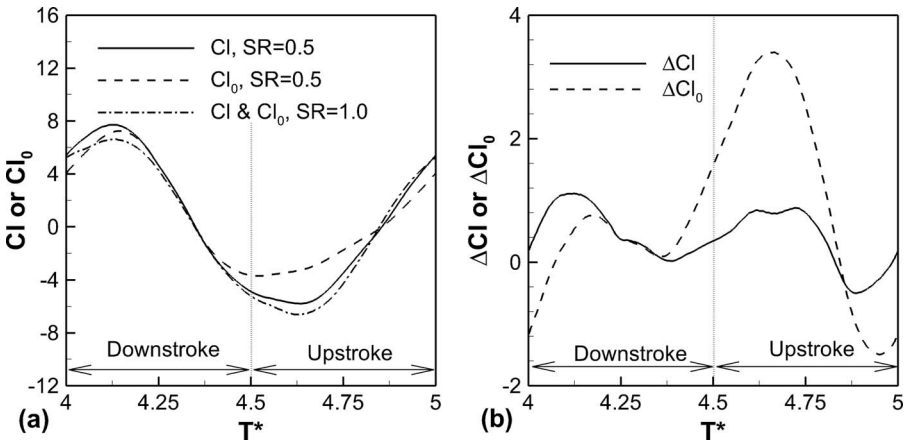

FIG. 3. The time histories of (a) Cl and Cl_0, (b) ΔCl and ΔCl_0 in one period in the cases of $SR = 0.5$ and $SR = 1.0$ for $\phi = \pi/2$, $St = 0.3$, $A^* = 0.25$, and $\alpha = 0^o$.

during the downstroke is similar to that in the $SR = 0.5$ case, except that the maximum of $Cl_0(t)$ is about 8% smaller. However, unlike the $SR = 0.5$ case, the minimum of $Cl_0(t)$ is reached when the wing is at about 1/3 of the upstroke. The peak magnitude of the negative $Cl_0(t)$ in the upstroke is equal to that of the positive $Cl_0(t)$ in the downstroke. In contrast to the case of $SR = 0.5$, this symmetric heaving kinematics without stretching and retracting wingspan in the downstroke and upstroke results in $\langle Cl_0 \rangle_T = 0$.

Figure 3(b) shows the time histories of the lift coefficient increments $\Delta Cl_0(t)$ and $\Delta Cl(t)$ defined in Eqs. (7) and (8). The flapping wing generates a large positive lift increment ($\Delta Cl_0 > 0$) in about 2/3 of the upstroke period for $SR = 0.5$, which is mainly caused by both retracting the wingspan during the upstroke and altering the vortical structures associated with the spanwise motion. During the most time of the downstroke, $\Delta Cl_0(t)$ remains positive although its value is relatively small. It is found that $\Delta Cl(t)$) is positive in the most time of both the upstroke and downstroke and there are two peaks in this period. This fact indicates that the additional lift enhancement is achieved by the effect of the morphing-altered flow structures. Furthermore, it is found that $\langle Cl_0 \rangle_T = \langle Cl \rangle_T = 0$ for $SR = 1.0$, $\langle Cl_0 \rangle_T = 0.81$, and $\langle Cl \rangle_T = 0.42$ for $SR = 0.5$. The time-averaged lift coefficient $\langle Cl \rangle_T = 0.42$ for $SR = 0.5$ is about half of $\langle Cl_0 \rangle_T = 0.81$. This further confirms that the contribution to the lift enhancement by the morphing-altered flow structures is comparable to that generated by changing the lifting surface area. Figure 4 shows the time-averaged lift coefficient increments $\langle \Delta Cl_0 \rangle_T$ and $\langle \Delta Cl \rangle_T$ as a function of SR for $\phi = \pi/2$, $St = 0.3$, $A^* = 0.25$, and $\alpha = 0^o$. The values

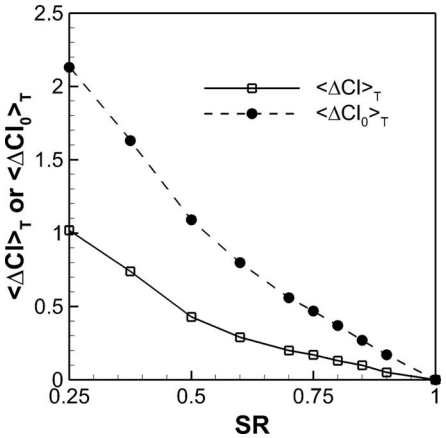

FIG. 4. The time-averaged increments of the lift coefficient $\langle \Delta Cl_0 \rangle_T$ and $\langle \Delta Cl \rangle_T$ as a function of the span ratio SR for $\phi = \pi/2$, $St = 0.3$, $A^* = 0.25$, and $\alpha = 0^o$.

of both $\langle \Delta Cl_0 \rangle_T$ and $\langle \Delta Cl \rangle_T$ are positive while they monotonically decay as SR increases, indicating that the lift enhancement is achieved for $0.25 \leq SR < 1$ and the lift enhancement is larger for a smaller value of SR.

B. Effects of other parameters

The time-averaged lift coefficient increments $\langle \Delta Cl_0 \rangle_T$ and $\langle \Delta Cl \rangle_T$ are evaluated in the parametric subspace (ϕ, St, A^*, α) for $AR_0 = 4$. Figure 5(a) shows $\langle \Delta Cl_0 \rangle_T$ and $\langle \Delta Cl \rangle_T$ as a function of the phase angle ϕ for $SR = 0.5$, $St = 0.3$, $A^* = 0.25$, and $\alpha = 0^o$. It is found that $\langle \Delta Cl_0 \rangle_T$ increases monotonically as ϕ increases and reaches the peak at $\phi = 90^o$. In contrast, $\langle \Delta Cl \rangle_T$ has the maximum at about $\phi = 0.39\pi$ ($\phi = 70^o$). Figure 5(b) shows $\langle \Delta Cl_0 \rangle_T$ and $\langle \Delta Cl \rangle_T$ as a function of the heaving amplitude A^* for $SR = 0.5$, $\phi = \pi/2$, $St = 0.3$, and $\alpha = 0^o$, which indicates the monotonic decay of $\langle \Delta Cl_0 \rangle_T$ as A^* increases and the presence of the maximum in $\langle \Delta Cl \rangle_T$ at $A^* = 0.375$. The dependencies of $\langle \Delta Cl_0 \rangle_T$ and $\langle \Delta Cl \rangle_T$ on the Strouhal number St are shown in Fig. 5(c) for $SR = 0.5$, $\phi = \pi/2$, $A^* = 0.25$, and $\alpha = 0^o$, which indicates the monotonic increase of $\langle \Delta Cl_0 \rangle_T$ as A^* increases and the presence of the maximum in $\langle \Delta Cl \rangle_T$ at $St = 0.4$. A preferred mode may exist in the subspace (ϕ, St, A^*, α) to achieve the maximum of $\langle \Delta Cl \rangle_T$, although the true global optimal mode is not known yet. Figure 5(d) shows that both $\langle \Delta Cl_0 \rangle_T$ and $\langle \Delta Cl \rangle_T$ weakly depend on the angle of attack α for $SR = 0.5$, $\phi = \pi/2$, $St = 0.3$, and $A^* = 0.25$.

Most importantly, the lift coefficient increment $\langle \Delta Cl \rangle_T$ in Fig. 5 is significantly larger than zero in all the cases. This indicates that the lift enhancement of the morphing wing is the phenomenon not just in a special case but also in a large domain in the parametric space. Therefore, the effect of the morphing-altered flow structures contributes significantly to the lift enhancement in addition to the effect of changing the wing area. As indicated in Sec. II B, there is a proportional relation $\langle \Delta Cl \rangle_T = C_{FS} \langle \Delta Cl_0 \rangle_T$, where the correlation coefficient C_{FS} is a function of the parameters (SR, ϕ, St, A^*, α). In all the cases, it is found that $0.3 \leq \langle \Delta Cl \rangle_T / \langle \Delta Cl_0 \rangle_T \leq 1$ depending on the parameters. This means that more than 30% of the overall lift enhancement is contributed by the effect of the morphing-altered flow structures. Although the main results for $AR_0 = L_{\max}/c = 4$ are presented in this paper, the lift enhancement for $AR_0 = 3 - 6$ is also studied. As shown in Fig. 5(e) for $SR = 0.5$, $\phi = \pi/2$, $St = 0.3$, $A^* = 0.25$, and $\alpha = 0^o$, it is found that $\langle \Delta Cl_0 \rangle_T$ and $\langle \Delta Cl \rangle_T$ are increased linearly with AR_0, and the slopes of the linear relations are 0.04 for $\langle \Delta Cl_0 \rangle_T$ and 0.027 for $\langle \Delta Cl \rangle_T$.

IV. FLOW STRUCTURES

A. General characteristics

To understand the physical mechanisms behind the lift enhancement associated with dynamically changing wingspan, the flow structures in the cases of $SR = 1.0$ and $SR = 0.5$ for (ϕ, St, A^*, α) = ($\pi/2$, 0.3, 0.25, 0^o) are investigated as the typical cases. The Q-criterion is used to identify the three-dimensional (3D) vortical structures, where Q is the second invariant of the velocity gradient tensor. The flow structures in the case of $SR = 1.0$ are examined as a reference where the wingspan remains unchanged. Then, the effects of stretching and retracting wingspan are studied by comparing the reference flow structures with those in the case of $SR = 0.5$.

The formation of the vortex rings in the near wake at five phases $T^* = 4.125$, 4.375, 4.625, 4.875, and 5.125 are shown in Fig. 6 that provide the top views of the flow structures. In the case of $SR = 1.0$, as shown in Fig. 6(a), the LEVs, trailing-edge vortices (TEVs), and tip vortices (TVs) generated at the beginning of the downstroke are denoted by LEV1, TEV1, TV1, and TV2, respectively. The detached LEVs in the previous downstroke and upstroke are denoted by PLEV1 and PLEV2, respectively. As indicated in Fig. 6(b), LEV1, TV1, and TV2 are generated and attached to the wing, while TEV1 sheds from the trailing edge in the downstroke. LEV1 has the positive spanwise vorticity, contributing to the positive vortex lift. Subsequently, new vortices LEV2, TEV2, TV3, and TV4 are generated during the reversal transition from the downstroke to the upstroke, and LEV1, TV1, and TV2 generated during the downstroke shed from the wing surface. As shown in

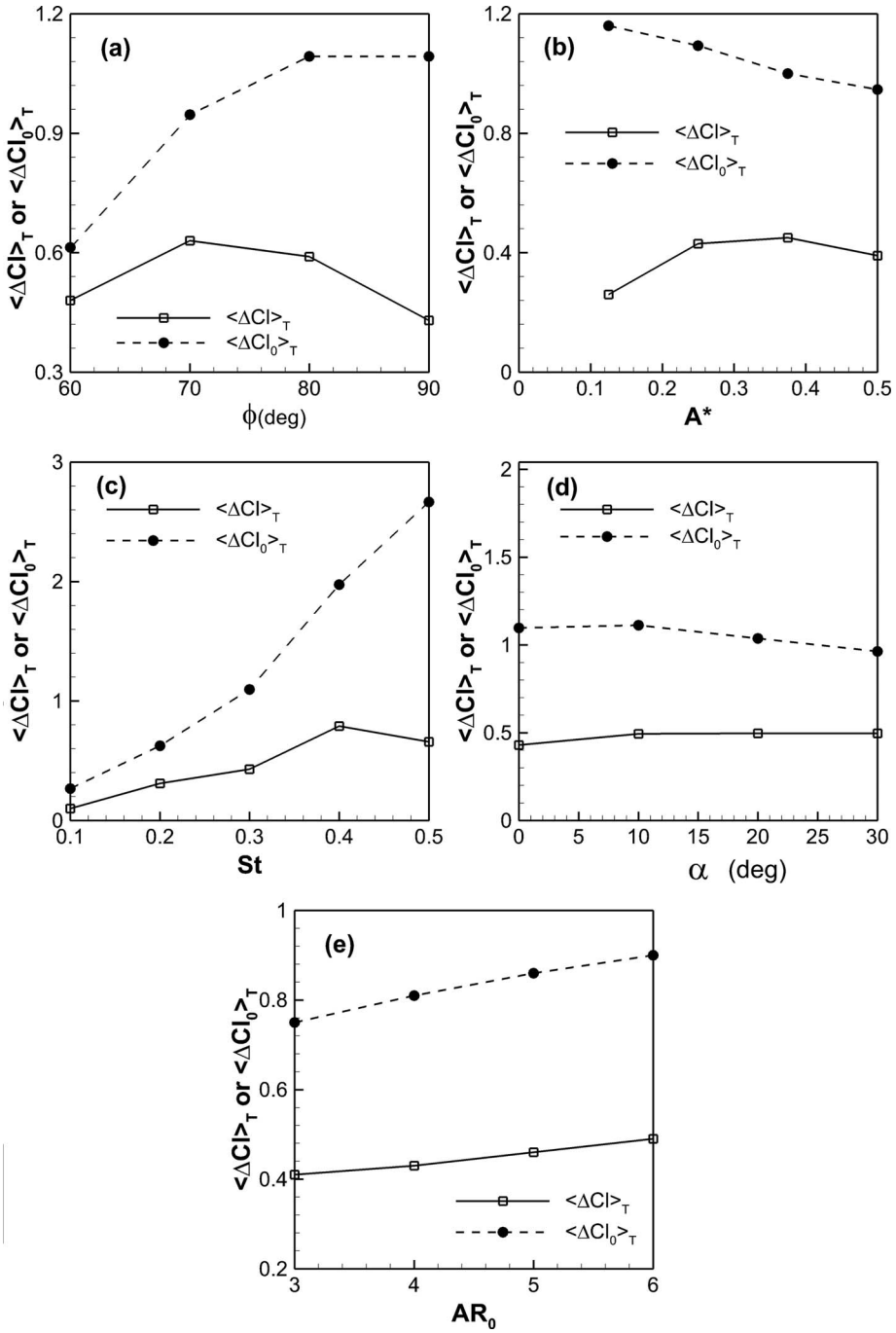

FIG. 5. The time-averaged increments of the lift coefficient $\langle \Delta Cl \rangle_T$ and $\langle \Delta Cl_0 \rangle_T$ as a function of the relevant parameters: (a) the phase difference for $SR = 0.5$, $St = 0.3$, $A^* = 0.25$, $\alpha = 0^o$; (b) flapping amplitude for $SR = 0.5$, $\phi = \pi/2$, $St = 0.3$, $\alpha = 0^o$; (c) Strouhal numbers for $SR = 0.5$, $\phi = \pi/2$, $A^* = 0.25$, $\alpha = 0^o$; (d) AoA for SR = 0.5, $\phi = \pi/2$, $St = 0.3$, and $A^* = 0.25$; and (e) AR_0 for $SR = 0.5$, $\phi = \pi/2$, $St = 0.3$, $A^* = 0.25$, and $\alpha = 0^o$. Note that $AR_0 = 4$ for (a)–(d).

Fig. 6(c), TEV1, TEV2, TV1, and TV2 together form the vortex ring R1. The detached vortex LEV1 stays near the upper surface of the wing and travels to the downstream, as shown in Figs. 6(c)–6(e).

In the case of $SR = 0.5$, the evolution of the flow structures is similar. At the beginning of the downstroke, as shown in Fig. 6(a), the vortices LEV1, TEV1, TV1, and TV2 are generated, and the vortices PLEV1 and PLEV2 are elongated due to the spanwise wing stretching. The vortex LEV1

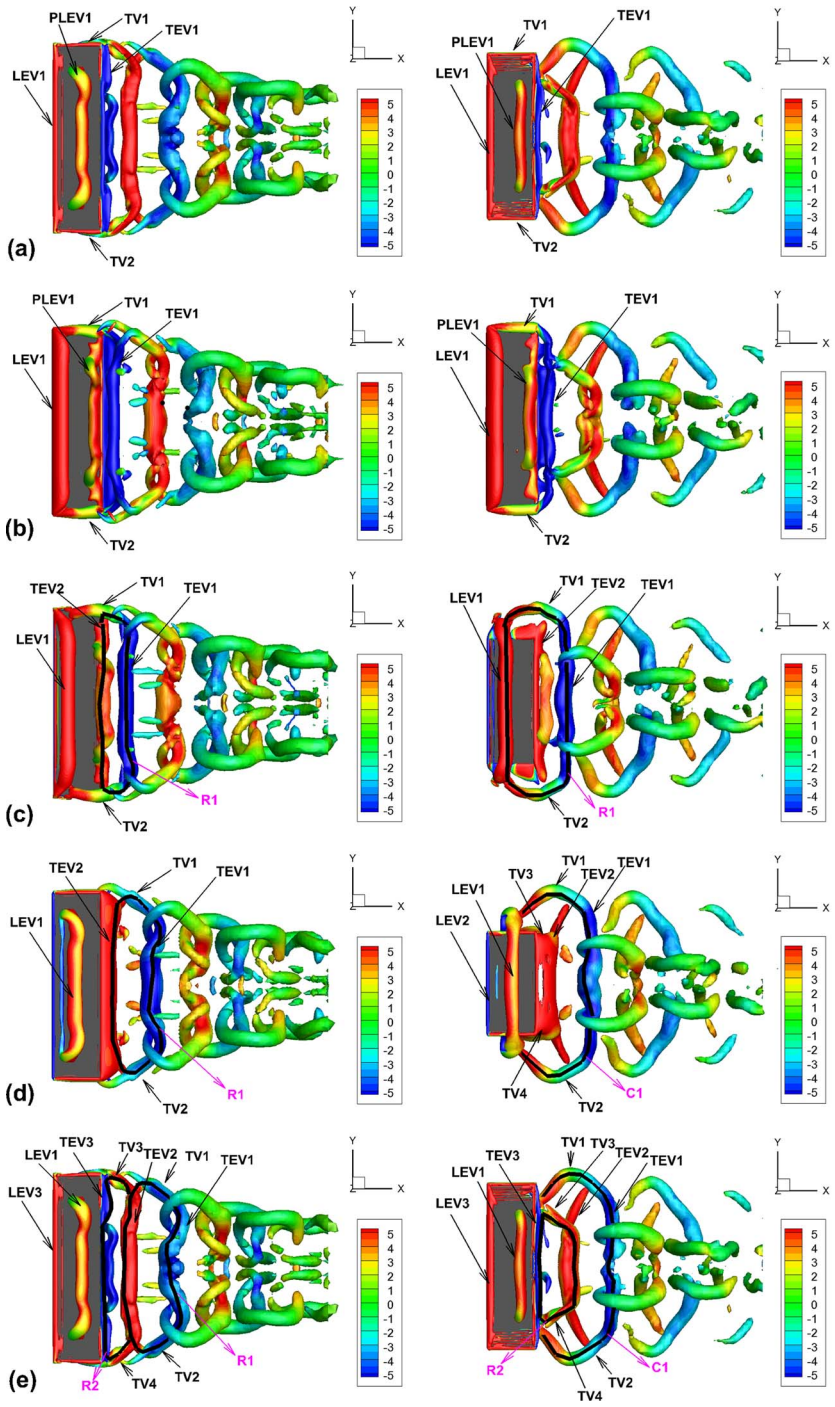

FIG. 6. The three-dimensional flow structures viewed from the top in the cases of $SR = 1.0$ (left) and $SR = 0.5$ (right) at different times (a) $T^* = 4.125$, (b) $T^* = 4.375$, (c) $T^* = 4.625$, (d) $T^* = 4.875$, and (e) $T^* = 5.125$. The iso-surface of $Q = 3.0$ is shown, where the gray scale (color online) indicates the spanwise vorticity. The detailed parameters for the cases of $SR = 1.0$ and $SR = 0.5$ are $(SR, \phi, St, A^*, \alpha) = (1.0, \pi/2, 0.3, 0.25, 0^o)$ and $(SR, \phi, St, A^*, \alpha) = (0.5, \pi/2, 0.3, 0.25, 0^o)$, respectively.

is also elongated and attached to the leading edge during the downstroke. The vortex TEV1 sheds from the trailing edge shortly after the beginning of the downstroke. The vortices TV1 and TV2 start to shed at the middle of the downstoke due to the retraction of the wingspan in this case, which is different from the case of $SR = 1.0$ where TV1 and TV2 shed at the end of the downstroke. At

the reversal transition from the downstroke to the upstroke, as shown in Fig. 6(c), LEV1 sheds from the leading edge, and then TEV1, LEV1, TV1, and TV2 together form the vortex ring R1 during this reversal. It is noticed that TV1 and TV2 are not connected to the newly generated TEV2. After shedding from the leading edge, LEV1 stays near the upper surface of the wing, contributing the positive vortex lift. Therefore, the vortex capture mechanism also exists during the downstroke in this case of $SR = 0.5$.

B. Vortex capture and stretching

Figure 7 shows the contours of the spanwise vorticity in the symmetrical plane $y = 0$ in the cases of $SR = 1.0$ and $SR = 0.5$ at the phases $T^* = 4.125$, $T^* = 4.375$, $T^* = 4.625$, $T^* = 4.875$, and $T^* = 5.125$. In both the cases, the vortex LEV1 is generated, and the vortex PLEV1 is trapped near the upper surface of the wing for about 1.5 periods, which contributes to the generation of the positive vortex lift until it merges with TEV2. This is referred to as the vortex capture mechanism in flapping flight, which is similar to the capture of a free vortex on an airfoil.[44–46] In 2D, although a free vortex cannot be stabilized near a stationary airfoil, vortex capture seems feasible on a moving wing with the right kinematics in a certain period. This phenomenon also occurs in the hovering flight of insects.[7,9,10] To compare the vortex stretching mechanism in the cases of $SR = 1.0$ and $SR = 0.5$, the top-viewed iso-surfaces of the spanwise vortex stretching term $\omega_y \partial u_y/\partial y$ at $T^* = 4.625$ in the upstroke are shown in Fig. 8 for $\phi = \pi/2$, $St = 0.5$, $A^* = 0.25$, and $\alpha = 0^\circ$. In the case of $SR = 0.5$, it is found that the vortex LEV1 near the upper surface is consistently intensified by the spanwise vortex stretching, which is supported by the correlations between the time histories of the integrated spanwise vortex stretching, vorticity, and wing motion shown in Fig. 11(a). The intensified vortex LEV1 contributes to the larger positive vortex lift even though it is shorter, which is further confirmed by the calculation of the vortex lift in the upstroke in Sec. V.

On the lower surface, the vortex PLEV2 generated in the previous cycle stays for about 1.5 periods near the lower surface of the wing. However, PLEV2 has the negative spanwise vorticity, which contributes to the negative vortex lift as the negative vortex capture. More interestingly, as shown in Figs. 7(c)–7(e), the vortex PLEV2 originated from the previous upstroke on the lower surface in the case of $SR = 0.5$ is much weaker than that in the case of $SR = 1.0$. This weaker PLEV2 is related to dynamically stretching and retracting wingspan. To observe the detailed 3D structure of PLEV2, the development of PLEV2 on the lower surface in the case of $SR = 0.5$ is shown in Fig. 9 in comparison with that in the case of $SR = 1.0$ as a reference. PLEV2 generates at $T^* = 3.5$, and part of PLEV2 sheds during $T^* = 3.5 - 4.0$ in the upstroke due to the retracting wingspan. In the upstroke, PLEV2 for $SR = 0.5$ is much shorter than that for $SR = 1.0$. Therefore, the total contribution of PLEV2 to the negative lift in the case of $SR = 0.5$ is smaller than that in the case of $SR = 1.0$. As the wing moves downward after $T^* = 4.0$, as shown in Fig. 9(c), PLEV2 sheds from the lower surface of the wing with several legs, and it deforms into streamwise stripes downstream. Due to this vorticity redistribution, the spanwise vorticity of PLEV2 is smaller in the downstroke. Figure 10 shows the bottom-viewed iso-surfaces of the spanwise vortex stretching term $\omega_y \partial u_y/\partial y$ in the cases of $SR = 1.0$ and $SR = 0.5$ at $T^* = 4.0$ (the end of the upstroke) for $St = 0.5$, $\phi = \pi/2$, $A^* = 0.25$, and $\alpha = 0^\circ$. The spanwise vortex stretching on the lower surface in the case of $SR = 0.5$ is highly 3D, which corresponds to the complicated 3D vortical structures observed in Fig. 9.

To quantitatively evaluate the correlation between the spanwise vortex stretching and wingspan motion in a flapping period, the two volume integrals of the spanwise vortex stretching term on the upper and lower surfaces around the LEVs are evaluated, which are defined as

$$[S_y]_{upper} \approx \int_{D_{upper}} \omega_y^* \frac{\partial u_y^*}{\partial y^*} dV^*, \quad [S_y]_{lower} \approx \int_{D_{lower}} \omega_y^* \frac{\partial u_y^*}{\partial y^*} dV^*, \tag{10}$$

where D_{upper} and D_{lower} are the selected domains $[-5, 0.5] \times [-3, 3] \times [z_w^*, 14]$ and $[-5, 0.5] \times [-3, 3] \times [-14, z_w^*]$ on the upper and lower surfaces, respectively, to include the spanwise vorticity near the LEVs and exclude the vorticity in the wake. Here the superscript * denotes the non-dimensional quantities. Similarly, the strengths of the spanwise vorticity in the two domains

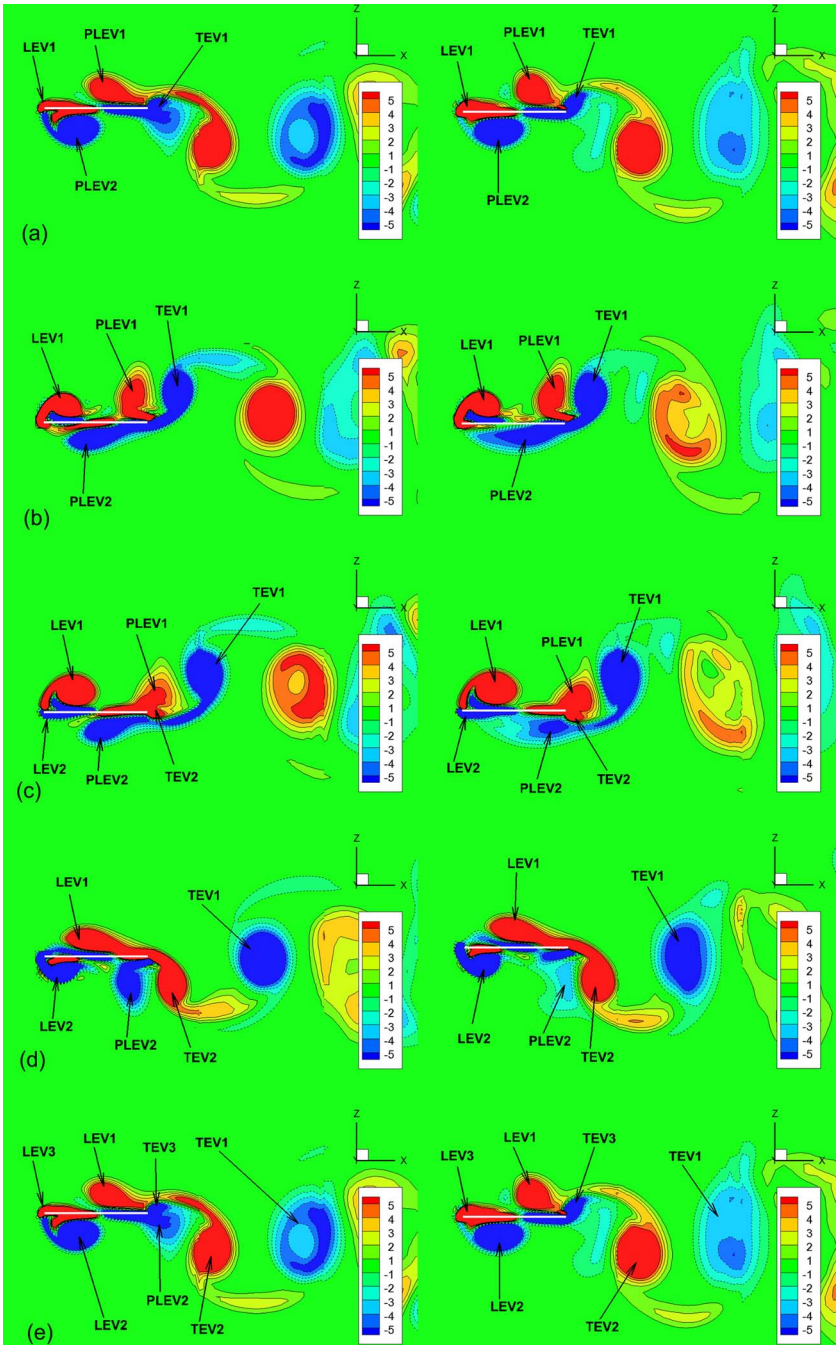

FIG. 7. The contours of the spanwise vorticity in $y = 0$ in the cases of $SR = 1.0$ (left) and $SR = 0.5$ (right) at different time (a) $T^* = 4.125$, (b) $T^* = 4.375$, (c) $T^* = 4.625$, (d) $T^* = 4.875$, and (e) $T^* = 5.125$. The detailed parameters for the cases of $SR = 1.0$ and $SR = 0.5$ are $(SR, \phi, St, A^*, \alpha) = (1.0, \pi/2, 0.3, 0.25, 0^o)$ and $(SR, \phi, St, A^*, \alpha) = (0.5, \pi/2, 0.3, 0.25, 0^o)$, respectively.

are given by $\lfloor\omega_y\rfloor_{upper}$ and $\lfloor\omega_y\rfloor_{lower}$. The spanwise wing motion is characterized by the spanwise velocity v_M of a middle point on the wing surface between the wing root and tip. Figure 11 shows the time histories of $\lfloor\omega_y\rfloor$, $\lfloor S_y\rfloor$, and v_M in a flapping period in the case of $SR = 0.5$. On the upper surface, as indicated in Fig. 11(a), the integrated spanwise vortex stretching $\lfloor S_y\rfloor$ is well correlated with v_M charactering the spanwise wing motion. In contrast, on the lower surface, there is a phase shift of 180° between $\lfloor S_y\rfloor$ and v_M as shown in Fig. 11(b). The magnitude of $\lfloor\omega_y\rfloor_{upper}$ (>0) is larger

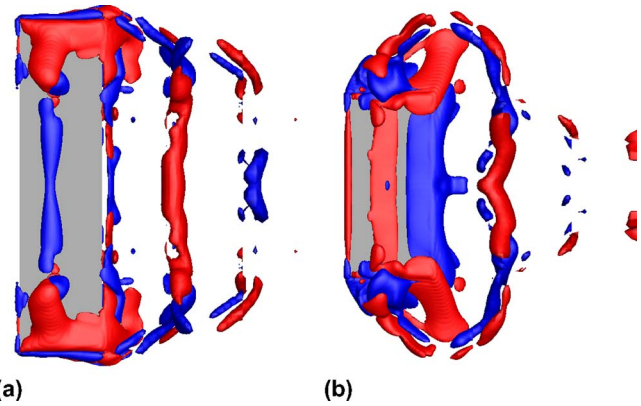

FIG. 8. The top-viewed iso-surfaces of the spanwise vortex stretching term $\omega_y \partial u_y/\partial y$ in the cases of (a) $SR = 1.0$ and (b) $SR = 0.5$ at $T^* = 4.625$ in the upstroke for $\phi = \pi/2$, $St = 0.5$, $A^* = 0.25$, and $\alpha = 0^o$. The light gray color (red) shows the iso-surfaces of $\omega_y \partial u_y/\partial y = 8$, indicating the regions where the vortices are stretched. The dark gray color (blue) shows the iso-surfaces of$\omega_y \partial u_y/\partial y = -8$, indicating the regions where the vortices are compressed.

than that of $\lfloor \omega_y \rfloor_{lower}$ (<0) in the most of the downstroke and the first 1/3 of the upstroke, which leads to the over vortex lift enhancement.

Based on the above observations, the LEVs on the upper surface are significantly intensified by the spanwise vortex stretching associated with dynamically changing wingspan, which contributes to the elevated lift in the case of $SR = 0.5$. In the meantime, the shorter and weaker LEVs on the lower surface in the upstroke have the smaller contribution to the negative lift. The combined effect of these mechanisms results in the overall vortex lift enhancement that corresponds to the peak in ΔCl in Fig. 3(b) in the upstroke in the case of $SR = 0.5$. The large peak in ΔCl_0 in the upstroke includes the contribution from the effect of changing the wing area. In the downstroke, since the vortical structures on the lower surface become highly 3D, the spanwise vorticity of these structures is decreased. As a result, they have a smaller contribution to the negative lift, which leads to the smaller peak in ΔCl in Fig. 3(b) in the downstroke.

V. LIFT DECOMPOSITION: VORTEX FORCE AND ACCELERATION

The lift decomposition is used to further understand the relationship between the lift enhancement and the flow structures. For a sufficiently large rectangular control domain in which a wing is enclosed, Wang *et al.*[47] gave a simple but reasonably accurate lift formula

$$L \approx \rho \boldsymbol{k} \cdot \int_{V_f} \boldsymbol{u} \times \boldsymbol{\omega}\, dV - \rho \boldsymbol{k} \cdot \int_{V_f} \frac{\partial \boldsymbol{u}}{\partial t} dV, \tag{11}$$

where V_f denotes the control volume, $\boldsymbol{k}$ is the unit vector normal to the freestream, $(\boldsymbol{u} \times \boldsymbol{\omega}) \cdot \boldsymbol{k}$ is the vertical component of the Lamb vector, and $\boldsymbol{u} \cdot \boldsymbol{k}$ is the vertical component of the velocity. The first and second terms in the right-hand side of Eq. (11) are the vortex lift (the Lamb vector integral) and the contribution associated with the fluid acceleration induced by a moving wing for the unsteady inertial effect.

To investigate the roles of the flow structures in the lift generation, a rectangular control volume of $[-5, 0.5] \times [-3, 3] \times [-14, 14]$ in the streamwise, spanwise, and vertical directions is selected. The lift coefficient Cl is used as a measure for the lift enhancement associated with the altered flow structures since the effect of changing the wing area is excluded in Cl. Figure 12 shows the lift coefficient Cl_{simp} calculated by using Eq. (11) compared with Cl calculated based on the pressure and viscous stress fields on the wing. The contributions from the vortex lift and the acceleration term are denoted by Cl_{vort} and Cl_{acc}, respectively. As shown in Fig. 12, Cl_{simp} is in good agreement with Cl. In the case of $SR = 0.5$, the time-averaged lift coefficient calculated by using the simple lift formula is 0.43, which agrees with 0.42 given by calculation based on the pressure and viscous stress

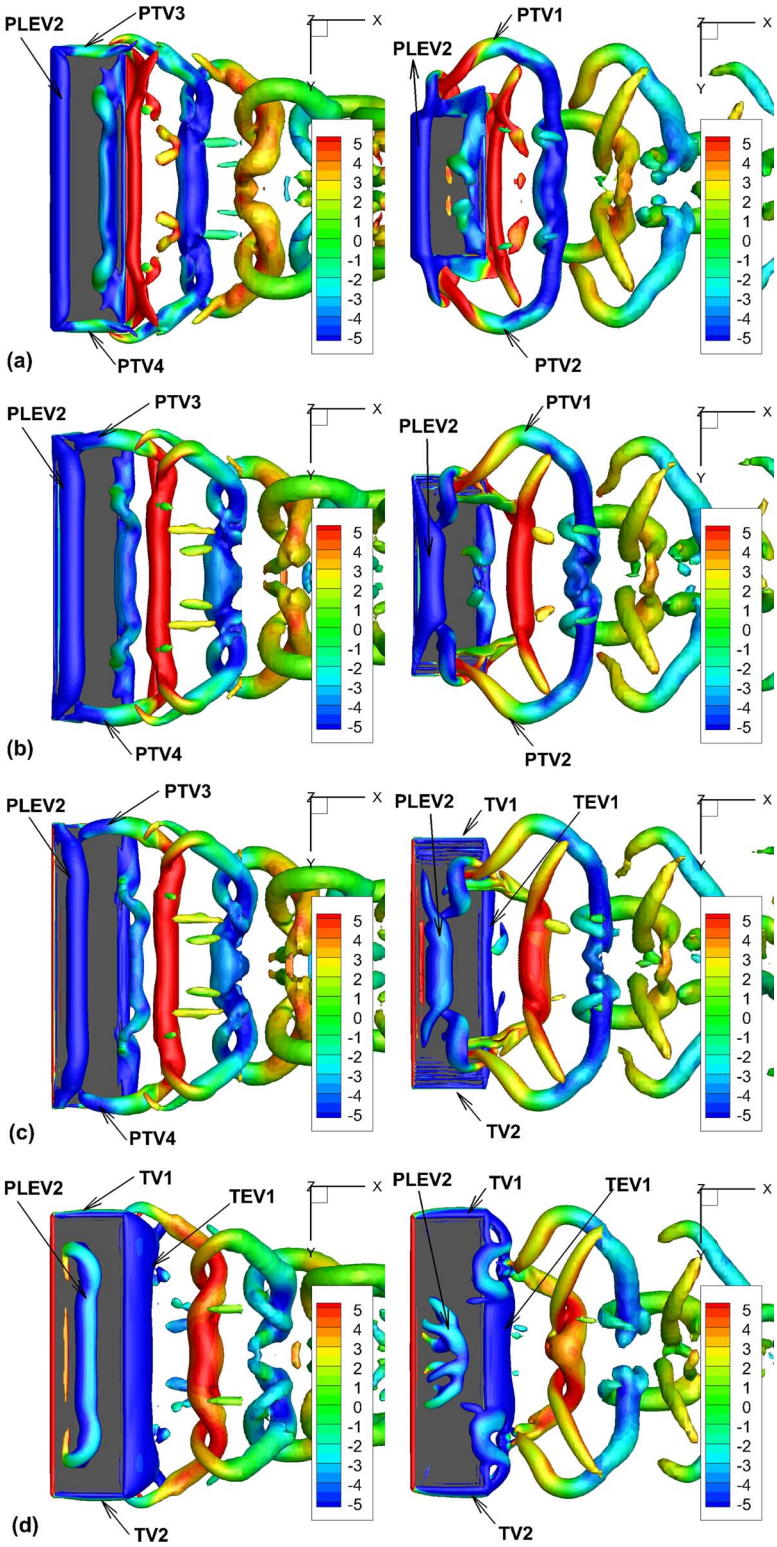

FIG. 9. The development of LEVs on the lower surface viewed from the bottom at (a) $T^* = 3.75$ and (b) $T^* = 4.0$ in the upstroke, and (c) $T^* = 4.125$ and (d) $T^* = 4.375$ in the downstroke. The left column: $SR = 1.0$, and the right column: $SR = 0.5$. The iso-surfaces of $Q = 3.0$ are shown, and the gray scale (color online) indicates the spanwise vorticity. The detailed parameters for the cases of $SR = 1.0$ and $SR = 0.5$ are $(SR, \phi, St, A^*, \alpha) = (1.0, \pi/2, 0.3, 0.25, 0^o)$ and $(SR, \phi, St, A^*, \alpha) = (0.5, \pi/2, 0.3, 0.25, 0^o)$, respectively.

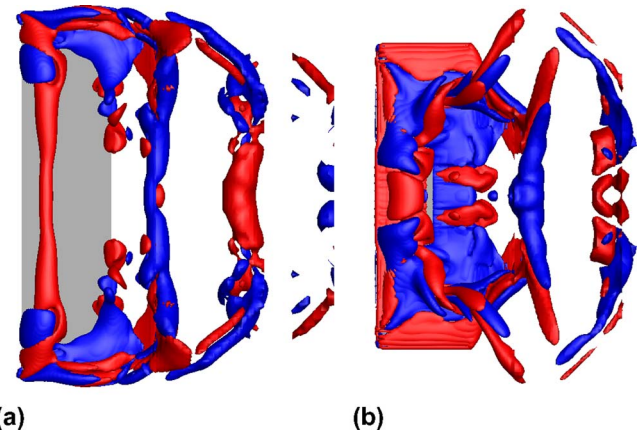

FIG. 10. The bottom-viewed iso-surfaces of the spanwise vortex stretching term $\omega_y \partial u_y/\partial y$ in the cases of (a) $SR = 1.0$ and (b) $SR = 0.5$ at $T^* = 4.0$ (the end of the upstroke) for $\phi = \pi/2$, $St = 0.5$, $A^* = 0.25$, and $\alpha = 0^o$. The light gray color (red) shows the iso-surfaces of$\omega_y \partial u_y/\partial y = 8$, indicating the regions where the vortices are stretched. The dark gray color (blue) shows the iso-surfaces of $\omega_y \partial u_y/\partial y = -8$, indicating the regions where the vortices are compressed.

fields on the wing surface. The relative error is about 2.4%. For the case of $SR = 1.0$, the positive lift and negative lift generated in the flapping are canceled out each other due to the symmetrical flapping motion such that the time-averaged lift coefficients $\langle Cl \rangle_T$ and $\langle Cl_{simp} \rangle_T$ are zero.

Figure 13 shows the contributions of the vortex lift term (ΔCl_{vort}) and local acceleration term (ΔCl_{acc}) to the lift coefficient increment ΔCl in one period. It is indicated that the contribution of the vortex lift to ΔCl is positive in a full period particularly in the upstroke. This means that the vortex lift is enhanced by dynamically stretching and retracting wingspan in flapping flight. In this case, the local acceleration term has the negative contribution to ΔCl particularly in the upstroke. Furthermore, the contributions of the vortical structures to Cl in the upper and lower portions of the control volume divided by the flat-plate rectangular wing are evaluated in the cases of $SR = 0.5$ and $SR = 1.0$. Figure 14 shows the contributions of the vortex lift term to Cl in the upper and lower portions of the control volume in one period. In the average sense, the contributions of the vortex lift term in the upper and lower portions to Cl are positive and negative, respectively, in the cases of $SR = 0.5$ and $SR = 1.0$. During the upstroke, the contributions of the vortex force in both the upper and lower portions for $SR = 0.5$ are larger than those for $SR = 1.0$. As pointed out in Sec. IV B, the LEVs on the upper surface in the upstroke are significantly intensified by the spanwise vortex

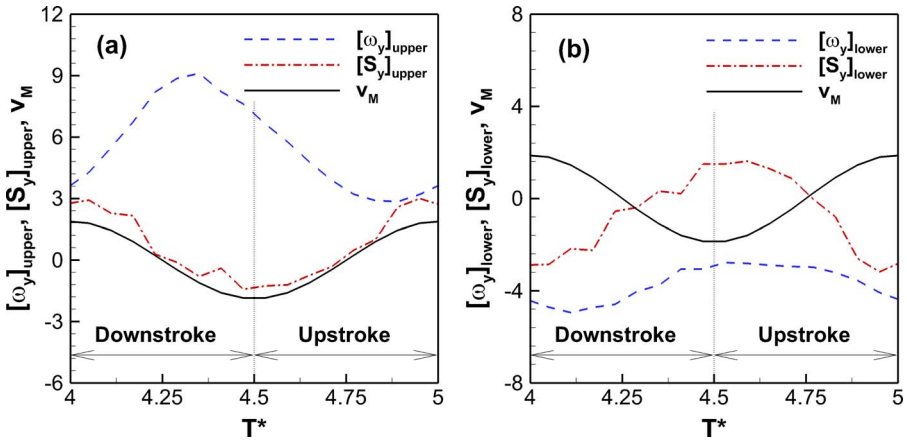

FIG. 11. The time histories of the integrated vortex stretching, vorticity, and spanwise motion velocity in a flapping period on (a) the upper surface and (b) the lower surface in the case of $SR = 0.5$.

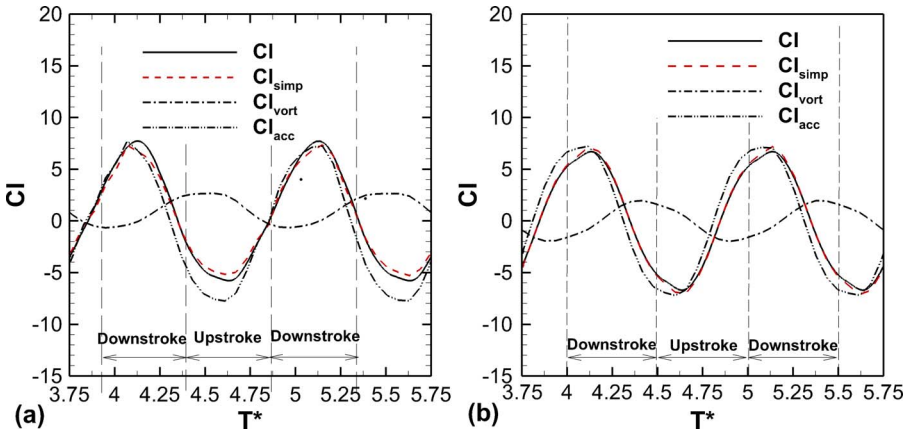

FIG. 12. . The decomposition of the lift coefficient in (a) $SR = 0.5$, and (b) $SR = 1.0$ for $\phi = \pi/2$, $St = 0.3$, $A^* = 0.25$, and $\alpha = 0^o$.

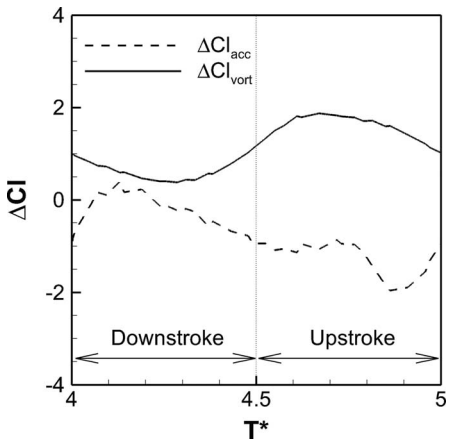

FIG. 13. The contributions of the Lamb vector term (the vortex force) and local acceleration term to the increment of the lift coefficient ΔCl in one period for $\phi = \pi/2$, $St = 0.3$, $A^* = 0.25$, and $\alpha = 0^o$.

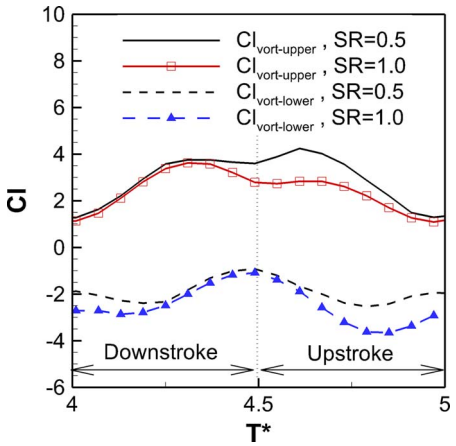

FIG. 14. The contributions of the Lamb vector term to the lift coefficient Cl in the upper and lower portions of the control volume for $\phi = \pi/2$, $St = 0.3$, $A^* = 0.25$, and $\alpha = 0^o$.

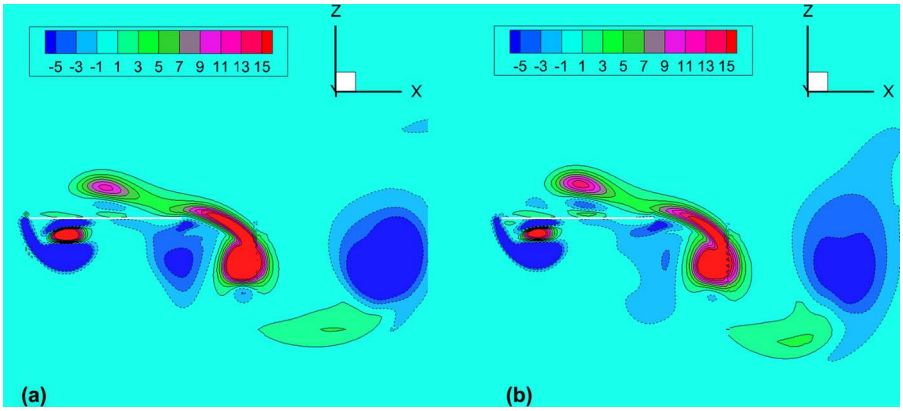

FIG. 15. The vertical component of the Lamb vector in the symmetrical plane $y = 0$ at $T^* = 4.875$ in the upstroke for (a) $SR = 1.0$ and (b) $SR = 0.5$ for $\phi = \pi/2$, $St = 0.3$, $A^* = 0.25$, and $\alpha = 0^o$.

stretching, which contributes to the elevated lift in the case of $SR = 0.5$. In the meantime, the shorter and more 3D LEVs on the lower surface have the smaller contribution to the negative lift. These differences lead to the higher positive peak in $\Delta Cl(t)$ during the upstroke in Fig. 3(b). During the downstroke, the contribution of the vortex force in the lower portion for $SR = 0.5$ is still larger than that for $SR = 1.0$. As a result, there is the smaller peak in $\Delta Cl(t)$ during the downstroke as indicated in Fig. 3(b). This is related to the vortical structures with the decreased spanwise vorticity on the lower surface as discussed in Sec. IV B. In summary, the vortex force associated with the vortical structures altered by dynamically changing wingspan significantly contributes the lift enhancement.

To visualize the contributions of the vortical structures to the lift enhancement, the instantaneous contours of the Lamb vector projected in the vertical direction at $T^* = 4.875$ (when the wing is near the end of the upstroke) are shown in Fig. 15. The positive vertical component of the Lamb vector associated with the intensified vortical structures on the upper surface is increased in the case of $SR = 0.5$. On the lower surface, as shown in Fig. 15(b), the negative vertical component of the Lamb vector in the case of $SR = 0.5$ has a smaller magnitude than that in the case of $SR = 1.0$. This corresponds to the vortex PLEV2 having the much smaller spanwise vorticity as shown in Fig. 7(d). Therefore, the vortical structures are altered by dynamically stretching and retracting wingspan, which contribute the elevated time-averaged lift.

VI. CONCLUSIONS

The flapping flat-plate rectangular wing with a dynamically stretching and retracting wingspan is studied through numerical simulations as a model of biologically inspired morphing wing for lift enhancement. The wingspan varies as a given function of time in a flapping cycle. The detailed flow fields and unsteady lift of the wing at the Reynolds number of 300 are calculated in the parametric space consisting of the span ratio, phase angle, Strouhal number, heaving amplitude, and geometrical angle of attack. It is found that the lift is significantly enhanced by dynamically stretching and retracting wingspan in flapping flight. The lift enhancement is achieved by both the effect of changing the wing area and the effect of the morphing-altered flow structures. It is observed that the LEVs on the upper surface in the upstroke are significantly intensified by the spanwise vortex stretching associated with the dynamically changing wingspan, which contributes the more positive vortex lift. At the meantime, the shorter and weaker LEVs on the lower surface in both the upstroke and downstroke have the smaller contribution to the negative lift. A combination of these mechanisms leads to the overall vortex lift enhancement in the upstroke and downstroke. The relationship between the lift enhancement and the morphing-altered flow structures is further confirmed by the lift decomposition into the vortex lift and the local acceleration term. This work reveals the significance of the dynamic wing morphing in the lift enhancement. Birds and bats could dynamically stretch and retract the wingspan in flapping flight for enhancing the lift unlike insects

with the fixed wingspan. This illustrates a fundamentally different aerodynamic aspect between birds/bats and insects in flapping flight.

ACKNOWLEDGMENTS

This work was supported by the National Natural Science Foundation of China under Project Nos. 10872201, 11232011, 11302238, and 11372331, and the National Basic Research Program of China under Project No. 2013CB834100 (Nonlinear science). Tianshu Liu would like to acknowledge the hospitality received at LNM during his visit, where he accomplished this work. The simulations were performed on TianHe-1. The authors would like to acknowledge the support from National Supercomputer Center in Tianjin. In addition, we would like to thank the reviewer for his/her constructive and meticulous comments.

[1] T. Weis-Fogh, "Quick estimates of flight fitness in hovering animals, including novel mechanisms for lift production," J. Exp. Biol. **59**(1), 169–230 (1973).
[2] F. O. Lehmann, S. P. Sane, and M. Dickinson, "The aerodynamic effects of wing-wing interaction in flapping insect wings," J. Exp. Biol. **208**(16), 3075–3092 (2005).
[3] C. P. Ellington, C. van den Berg, A. P. Willmott, and A. L. R. Thomas, "Leading-edge vortices in insect flight," Nature (London) **384**(6610), 626–630 (1996).
[4] H. Liu, C. P. Ellington, K. Kawachi, C. Van den Berg, and A. P. Willmott, "A computational fluid dynamic study of hawkmoth hovering," J. Exp. Biol. **201**(4), 461–477 (1998).
[5] R. J. Bomphrey, "The aerodynamics of manduca sexta: Digital particle image velocimetry analysis of the leading-edge vortex," J. Exp. Biol. **208**(6), 1079–1094 (2005).
[6] T. Maxworthy, "The formation and maintenance of a leading-edge vortex during the forward motion of an animal wing," J. Fluid Mech. **587**, 471–475 (2007).
[7] D. Lentink and M. H. Dickinson, "Rotational accelerations stabilize leading edge vortices on revolving fly wings," J. Exp. Biol. **212**(16), 2705–2719 (2009).
[8] M. Sun and J. Tang, "Unsteady aerodynamic force generation by a model fruit fly wing in flapping motion," J. Exp. Biol. **205**(1), 55–70 (2002).
[9] M. H. Dickinson, "The effects of wing rotation on unsteady aerodynamic performance at low Reynolds-numbers," J. Exp. Biol. **192**, 179–206 (1994).
[10] M. H. Dickinson, F. O. Lehmann, and S. P. Sane, "Wing rotation and the aerodynamic basis of insect flight," Science **284**(5422), 1954–1960 (1999).
[11] H. Huang and M. Sun, "Dragonfly forewing-hindwing interaction at various flight speeds and wing phasing," AIAA J. **45**(2), 508–511 (2007).
[12] C. T. Hsieh, C. F. Kung, C. C. Chang, and C. C. Chu, "Unsteady aerodynamics of dragonfly using a simple wing-wing model from the perspective of a force decomposition," J. Fluid Mech. **663**, 233–252 (2010).
[13] D. Rival, D. Schonweitz, and C. Tropea, "Vortex interaction of tandem pitching and plunging plates: A two-dimensional model of hovering dragonfly-like flight," Bioinspir. Biomimet. **6**(1), 016008 (2011).
[14] G. R. Spedding, M. Rosen, and A. Hedenstrom, "A family of vortex wakes generated by a thrush nightingale in free flight in a wind tunnel over its entire natural range of flight speeds," J. Exp. Biol. **206**(14), 2313–2344 (2003).
[15] A. Hedenstrom, L. C. Johansson, M. Wolf, R. von Busse, Y. Winter, and G. R. Spedding, "Bat flight generates complex aerodynamic tracks," Science **316**(5826), 894–897 (2007).
[16] A. Hedenstrom, L. C. Johansson, and G. R. Spedding, "Bird or bat: Comparing airframe design and flight performance," Bioinspir. Biomimet. **4**(1), 015001 (2009).
[17] T. Y. Hubel, N. I. Hristov, S. M. Swartz, and K. S. Breuer, "Time-resolved wake structure and kinematics of bat flight," Exp. Fluids **46**(5), 933–943 (2009).
[18] T. Y. Hubel, D. K. Riskin, S. M. Swartz, and K. S. Breuer, "Wake structure and wing kinematics: The flight of the lesser dog-faced fruit bat, *cynopterus brachyotis*," J. Exp. Biol. **213**(20), 3427–3440 (2010).
[19] D. L. Altshuler, R. Dudley, S. M. Heredia, and J. A. McGuire, "Allometry of hummingbird lifting performance," J. Exp. Biol. **213**(5), 725–734 (2010).
[20] M. Yu, Z. J. Wang, and H. Hu, "Formation of bifurcated wakes behind finite span flapping wings," AIAA J. **51**(8), 2040–2044 (2013).
[21] K. D. von Ellenrieder, K. Parker, and J. Soria, "Flow structures behind a heaving and pitching finite-span wing," J. Fluid Mech. **490**, 129–138 (2003).
[22] H. Dong, R. Mittal, and F. M. Najjar, "Wake topology and hydrodynamic performance of low-aspect-ratio flapping foils," J. Fluid Mech. **566**, 309–343 (2006).
[23] H. Hu, L. Clemons, and H. Igarashi, "An experimental study of the unsteady vortex structures in the wake of a root-fixed flapping wing," Exp. Fluids **51**(2), 347–359 (2011).
[24] K. D. von Ellenrieder and S. Pothos, "PIV measurements of the asymmetric wake of a two dimensional heaving hydrofoil," Exp. Fluids **44**(5), 733–745 (2008).
[25] Z. C. Zheng and Z. Wei, "Study of mechanisms and factors that influence the formation of vortical wake of a heaving airfoil," Phys. Fluids **24**(10), 103601 (2012).
[26] S. P. Sane, "The aerodynamics of insect flight," J. Exp. Biol. **206**(23), 4191–4208 (2003).

[27] S. Ho, H. Nassef, N. Pornsinsirirak, Y. C. Tai, and C. M. Ho, "Unsteady aerodynamics and flow control for flapping wing flyers," Prog. Aerospace Sci. **39**(8), 635–681 (2003).
[28] F. O. Lehmann, "The mechanisms of lift enhancement in insect flight," Naturwissenschaften **91**(3), 101–122 (2004).
[29] Z. J. Wang, "Dissecting insect flight," Annu. Rev. Fluid Mech. **37**(1), 183–210 (2005).
[30] P. R. Bandyopadhyay, "Swimming and flying in nature—The route toward applications: The freeman scholar lecture," J. Fluids Eng. **131**(3), 031801 (2009).
[31] T. Liu, J. Montefort, and S. Pantula, "Effects of flexible fin on low-frequency oscillation in post-stalled flows," AIAA J. **48**(6), 1235–1247 (2010).
[32] W. Shyy, H. Aono, S. K. Chimakurthi, P. Trizila, C. K. Kang, C. E. S. Cesnik, and H. Liu, "Recent progress in flapping wing aerodynamics and aeroelasticity," Prog. Aerospace Sci. **46**(7), 284–327 (2010).
[33] C. K. Kang, H. Aono, C. E. S. Cesnik, and W. Shyy, "Effects of flexibility on the aerodynamic performance of flapping wings," J. Fluid Mech. **689**, 32–74 (2011).
[34] M. J. Shelley and J. Zhang, "Flapping and bending bodies interacting with fluid flows," Annu. Rev. Fluid Mech. **43**(1), 449–465 (2011).
[35] L. Zhu, G. He, S. Wang, L. Miller, X. Zhang, Q. You, and S. Fang, "An immersed boundary method based on the lattice Boltzmann approach in three dimensions, with application," Comput. Math. Appl. **61**(12), 3506–3518 (2011).
[36] K. Shoele and Q. Zhu, "Leading edge strengthening and the propulsion performance of flexible ray fins," J. Fluid Mech. **693**, 402–432 (2012).
[37] T. S. Liu, K. Kuykendoll, R. Rhew, and S. Jones, "Avian wing geometry and kinematics," AIAA J. **44**(5), 954–963 (2006).
[38] M. Wolf, L. C. Johansson, R. von Busse, Y. Winter, and A. Hedenstrom, "Kinematics of flight and the relationship to the vortex wake of a Pallas' long tongued bat (Glossophaga Soricina)," J. Exp. Biol. **213**(12), 2142–2153 (2010).
[39] S. Barbarino, O. Bilgen, R. M. Ajaj, M. I. Friswell, and D. J. Inman, "A review of morphing aircraft," J. Intell. Mater. Syst. Struct. **22**, 823–877 (2011).
[40] C. S. Peskin, "The immersed boundary method," Acta Numer. **11**, 479–517 (2002).
[41] R. Mittal and G. Iaccarino, "Immersed boundary methods," Annu. Rev. Fluid Mech. **37**, 239–261 (2005).
[42] S. Z. Wang and X. Zhang, "An immersed boundary method based on discrete stream function formulation for two- and three-dimensional incompressible flows," J. Comput. Phys. **230**(9), 3479–3499 (2011).
[43] W. Chang, F. Giraldo, and B. Perot, "Analysis of an exact fractional step method," J. Comput. Phys. **180**(1), 183–199 (2002).
[44] P. G. Saffman and J. S. Sheffield, "Flow over a wing with an attached free vortex," Stud. Appl. Math. **57**(2), 107–117 (1977).
[45] M. K. Huang and C. Y. Chow, "Trapping of a free vortex by Joukowski airfoils," AIAA J. **20**(3), 292–298 (1982).
[46] C. Y. Chow, M. K. Huang, and C. Z. Yan, "Unsteady-flow about a Joukowski airfoil in the presence of moving vortices," AIAA J. **23**(5), 657–658 (1985).
[47] S. Z. Wang, X. Zhang, G. W. He, and T. S. Liu, "A lift formula applied to low-Reynolds-number unsteady flows," Phys. Fluids **25**, 093605 (2013).